

Attribution-NonCommercial-NoDerivatives 4.0 International (CC BY-NC-ND 4.0)
<https://creativecommons.org/licenses/by-nc-nd/4.0/>

Access to this work was provided by the University of Maryland, Baltimore County (UMBC) ScholarWorks@UMBC digital repository on the Maryland Shared Open Access (MD-SOAR) platform.

Please provide feedback

Please support the ScholarWorks@UMBC repository by emailing scholarworks-group@umbc.edu and telling us what having access to this work means to you and why it's important to you. Thank you.

Size-Specific Modulation of a Multienzyme Glucosome Assembly during the Cell Cycle

Miji Jeon, Danielle L. Schmitt, Minjoung Kyoung, and Songon An*

Cite This: <https://doi.org/10.1021/acsbiomedchemau.3c00037>

Read Online

ACCESS |



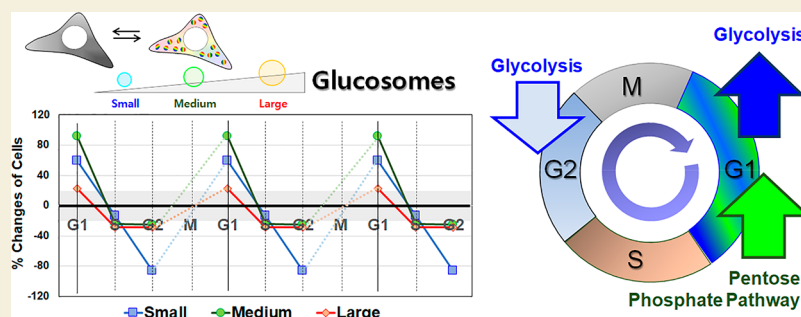
Metrics & More



Article Recommendations



Supporting Information



ABSTRACT: Enzymes in glucose metabolism have been subjected to numerous studies, revealing the importance of their biological roles during the cell cycle. However, due to the lack of viable experimental strategies for measuring enzymatic activities particularly in living human cells, it has been challenging to address whether their enzymatic activities and thus anticipated glucose flux are directly associated with cell cycle progression. It has remained largely elusive how human cells regulate glucose metabolism at a subcellular level to meet the metabolic demands during the cell cycle. Meanwhile, we have characterized that rate-determining enzymes in glucose metabolism are spatially organized into three different sizes of multienzyme metabolic assemblies, termed glucosomes, to regulate the glucose flux between energy metabolism and building block biosynthesis. In this work, we first determined using cell synchronization and flow cytometric techniques that enhanced green fluorescent protein-tagged phosphofructokinase is adequate as an intracellular biomarker to evaluate the state of glucose metabolism during the cell cycle. We then applied fluorescence single-cell imaging strategies and discovered that the percentage of Hs578T cells showing small-sized glucosomes is drastically changed during the cell cycle, whereas the percentage of cells with medium-sized glucosomes is significantly elevated only in the G1 phase, but the percentage of cells showing large-sized glucosomes is barely or minimally altered along the cell cycle. Should we consider our previous localization–function studies that showed assembly size-dependent metabolic roles of glucosomes, this work strongly suggests that glucosome sizes are modulated during the cell cycle to regulate glucose flux between glycolysis and building block biosynthesis. Therefore, we propose the size-specific modulation of glucosomes as a behind-the-scenes mechanism that may explain functional association of glucose metabolism with the cell cycle and, thereby, their metabolic significance in human cell biology.

KEYWORDS: Cell Cycle, Glucose Metabolism, Metabolic Adaptation, Glycolysis, Multienzyme Assembly, Fluorescence Live-Cell Imaging, Cancer Cell Metabolism

INTRODUCTION

Metabolism undergoes dynamic changes during the cell cycle to provide energy and building blocks for a cell to duplicate and divide.^{1–4} Based on extensive studies from yeast and unicellular eukaryotic cells,^{5,6} glucose metabolism, particularly glycolysis and the pentose phosphate pathway (PPP), is upregulated during the G1 phase. Their metabolic activities remain high during the S phase to support DNA replication. However, when DNA replication is completed in the G2 phase, glucose metabolism decreases to basal levels. At the same time, protein and lipid biosynthesis are promoted during the G2 phase. During mitosis, then, a cell divides into two daughter cells. The life cycle of eukaryotic cells continues as described when daughter cells reenter the cell cycle. However, it has

remained mostly elusive how multicellular eukaryotic cells, particularly human cells, regulate metabolic pathways to meet such metabolic demands during the cell cycle.^{5,6}

Nevertheless, metabolic interplays between enzymes in glucose metabolism and the cell cycle in human cells have been gradually disclosed.^{4–6} For instance, the expression of hexokinase 2 in human epithelial type 2 cells and cancer-

Received: June 9, 2023

Revised: July 26, 2023

Accepted: July 26, 2023

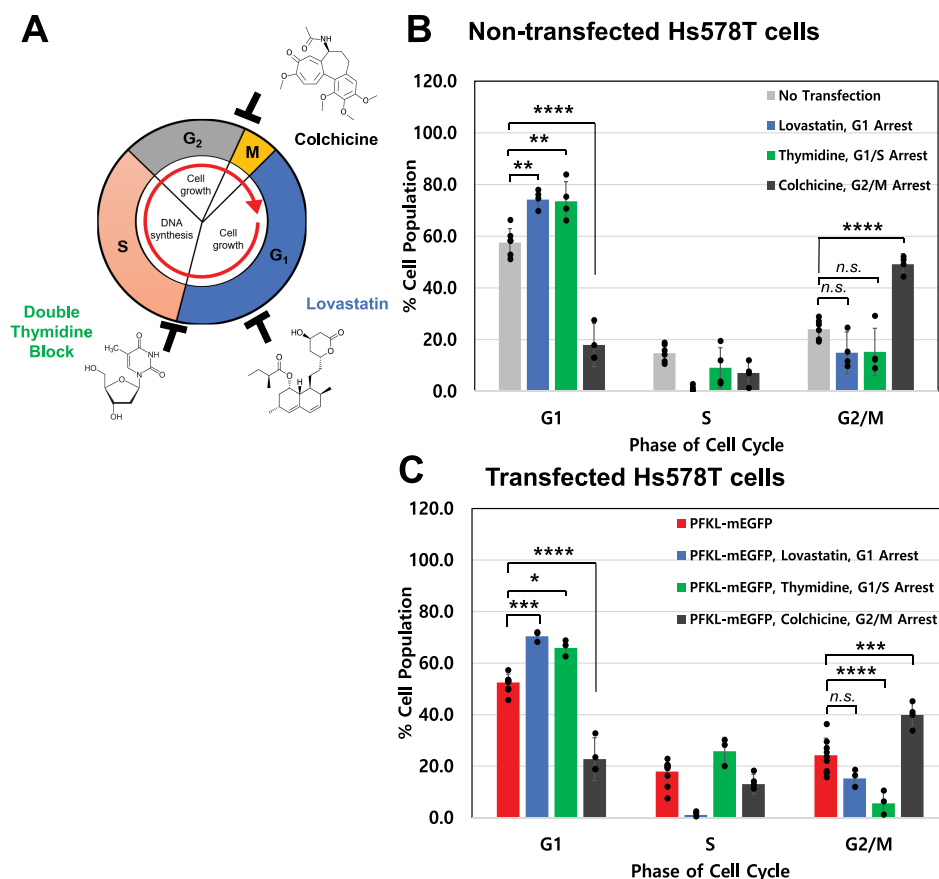


Figure 1. Small molecule-promoted cell synchronization with and without the expression of a glucosome marker in Hs578T cells. (A) Schematic diagram showing how small molecule-promoted cell synchronization is achieved during the cell cycle. (B, C) Population (%) changes of Hs578T cells at each phase of the cell cycle in the presence of a cell cycle inhibitor (i.e., lovastatin (blue, 40 μ M), thymidine (green, 2 mM), and colchicine (black, 100 nM)) without (B, $N_{\text{control}} = 6$, $N_{\text{lovastatin}} = 4$, $N_{\text{thymidine}} = 4$, $N_{\text{colchicine}} = 4$) and with (C, $N_{\text{control}} = 9$, $N_{\text{lovastatin}} = 3$, $N_{\text{thymidine}} = 3$, $N_{\text{colchicine}} = 4$) the expression of PFKL-mEGFP as a glucosome marker. Statistical analyses were performed using two-way ANOVA and Tukey's multiple comparison tests. Error bars represent standard deviations. Statistical significance is defined as $p < 0.05$ with a 95% confidence interval while n.s. refers to not significant. * $p < 0.05$, ** $p < 0.01$, *** $p < 0.001$, **** $p < 0.0001$.

associated fibroblasts was upregulated during the G1 phase.^{7,8} The expression level of 6-phosphofructo-2-kinase/fructose-1,6-bisphosphatase isoform 3 (PFKFB3), whose activity enables allosteric activation of phosphofructokinase 1 (PFK) for glycolysis, was also increased in the late G1 but decreased in the early S phase in human embryonic kidney cells, human breast cancer cells (MDA-MB-231 and MCF7), neuroblastoma cells (SHSY-5Y), and human cervical cancer cells (HeLa).^{9–12} However, other than their expression levels, no enzymatic activities of these and other enzymes in glycolysis or their impacts on glycolytic flux have been directly measured yet from human cells to link their functional participation in the cell cycle. Nonetheless, changes of enzymatic activity of glucose-6-phosphate dehydrogenase and its impact on glucose shunt to the PPP were measured, demonstrating the promotion of the PPP during the late G1 and the early S phase of the cell cycle in human colon adenocarcinoma cells (HT29).^{13,14} Otherwise, we barely understand how the intracellular activities of metabolic enzymes in glucose metabolism are functionally associated with governing the glucose flux during the cell cycle.

Meanwhile, we have identified that human liver-type phosphofructokinase 1 (PFKL) spatially forms various sizes of a cytoplasmic metabolic assembly, namely, the glucosome, and recruits at least three rate-determining enzymes in glucose

metabolism, including fructose-1,6-bisphosphatase, pyruvate kinase, and phosphoenolpyruvate carboxykinase 1.¹⁵ Due to the heterogeneity of the observed sizes of the glucosomes under fluorescence single-cell microscopy, we have subsequently categorized them into three subclasses for their functional characterization (i.e., small-, medium-, and large-sized glucosomes).¹⁵ Briefly, small-sized glucosomes are defined as having less than our calculated area of a point spread function for the emission of monomeric enhanced green fluorescent protein (mEGFP) (i.e., $\sim 0.1 \mu\text{m}^2$). Medium-sized glucosomes are then defined as having larger than $0.1 \mu\text{m}^2$ but less than $3 \mu\text{m}^2$ size. The $3 \mu\text{m}^2$ cutoff is experimentally determined based on our observation that noncancerous human cell lines we have tested do not display glucosomes that are larger than $3 \mu\text{m}^2$ in our growth conditions. Accordingly, large-sized glucosomes are defined to range from $3 \mu\text{m}^2$ to $8 \mu\text{m}^2$, which we have seen in various human cancer cell lines.¹⁵ Nevertheless, when fluorescent granules display larger size than $8 \mu\text{m}^2$ at single-cell levels, we have found that such aggregates are primarily composed of an immobile fraction of transfected enzymes and importantly their formation is apparently nonspecific to the identity of transfected enzymes.^{15,16} Fluorescent aggregates larger than $8 \mu\text{m}^2$ in size are not classified as glucosomes in our work. At the same time, others have also detected various sizes of spatial

assemblies of human PFKL, for example, in HepG2 cells by immunostaining¹⁷ as well as in transiently transfected rat breast cancer cells under fluorescence live-cell imaging,¹⁸ although these studies did not include other enzymes involved in glucose metabolism. Importantly, our localization–function studies primarily using high-content live-cell imaging assays^{15,19} as well as mathematical modeling analysis²⁰ have strongly suggested that small-sized glucosomes are responsible for regulating glycolysis whereas medium- and large-sized glucosomes shunt glucose flux preferentially into the PPP and serine biosynthesis, respectively. Therefore, we envision that glucosomes would be functionally associated with various biological processes, including the cell cycle, in human cells.

In this work, we investigated whether human cells modulate the size of glucosome assemblies at a subcellular level during the cell cycle by employing fluorescence live-cell imaging along with cell synchronization and flow cytometry. To begin with, we determined that transient introduction of PFKL-mEGFP as a glucosome marker to human triple-negative breast carcinoma Hs578T cells shows no significant influence on cell cycle progression and small molecule-mediated cell cycle synchronization. Then, our in-depth single-cell analyses have revealed that the percentage of cells displaying small-sized glucosomes is drastically changed during the cell cycle, whereas the percentage of cells showing medium-sized glucosomes is significantly elevated only in the G1 phase, but the percentage of cells exhibiting large-sized glucosomes is barely or minimally altered along the cell cycle. Taking into account of our previous localization–function studies that showed assembly size-dependent metabolic roles of glucosomes,^{15,19,20} this work reinforces the current understanding of metabolic demands at the G1 phase (i.e., the upregulation of glycolysis and the PPP). At the same time, this work suggests previously unrecognized metabolic demands at the G2 phase, involving the down-regulation of glycolysis but a relatively sustained glucose flux into the PPP and serine biosynthesis. Collectively, our single-cell analyses provide strong evidence that glucosome sizes are dynamically modulated during the cell cycle in a size-specific manner, inferring the metabolic significance of glucosomes and their dynamics in human cell biology.

RESULTS

Expression of an Intracellular Glucosome Marker for Cell Cycle Analysis

Recent studies have implicated phosphofructokinase as a scaffold of a multienzyme metabolic assembly for glucose metabolism in eukaryotic cells.^{15,17,18} Likewise, we have been using mEGFP-tagged human PFKL as an intracellular biomarker for glucosomes in living human cells.^{15,19–22} In this work, we started carrying out flow cytometry-assisted cell cycle analysis with asynchronized human Hs578T cells with and without the expression of PFKL-mEGFP. Our histogram analysis of asynchronous Hs578T cells showed that the percentage of cells in each phase of the cell cycle was statistically unchanged in the presence of PFKL-mEGFP (Supplemental Figure S1). Apparently, the expression of PFKL-mEGFP did not alter or negatively influence the overall distribution of Hs578T cells among the phases of the cell cycle. Therefore, we determined that subcellular dynamics of PFKL-mEGFP in living human cells would be adequate as an intracellular glucosome marker to investigate the state of glucose metabolism during the cell cycle.

Small Molecule-Promoted Cell Synchronization with a Glucosome Marker

We then investigated the cell cycle-dependent distribution of small molecule-treated Hs578T cells with and without a glucosome marker, PFKL-mEGFP (Figure 1). Note that we have previously demonstrated that >98% Hs578T cells show glucosomes when they are transfected with PFKL-mEGFP in our culture conditions.¹⁵

First, we treated Hs578T cells with lovastatin (40 μ M), which is known to arrest cells in the G1 phase through the inhibition of 3-hydroxy-3-methylglutaryl coenzyme A reductase (Figure 1A).^{23–28} Without the glucosome marker PFKL-mEGFP, the percentage of G1-arrested Hs578T cells increased 16.6% in the presence of lovastatin, relative to the percentage of asynchronous Hs578T cells in the G1 phase (i.e., $57.6 \pm 5.4\%$ to $74.2 \pm 3.5\%$) (Figure 1B, light gray vs blue). Meanwhile, lovastatin also increased by 17.9% PFKL-mEGFP-transfected Hs578T cells in the G1 phase, relative to the percentage of asynchronous Hs578T cells expressing PFKL-mEGFP (i.e., $52.5 \pm 3.2\%$ to $70.4 \pm 2.1\%$) (Figure 1C, red vs blue). These data support that the expression of the glucosome marker has no significant influence on arresting cells in the G1 phase by lovastatin (Figure 1, panel B vs C, blue).

Second, we also used a double thymidine block (2 mM) to arrest Hs578T cells in the G1/S phase transition (Figure 1A). Thymidine is capable of arresting cells at the G1/S boundary by blocking DNA replication.^{29,30} The treatment with thymidine promoted a 16.0% increase of nontransfected Hs578T cells in the G1 phase relative to the G1 population of asynchronous nontransfected Hs578T cells (i.e., $57.6 \pm 5.4\%$ to $73.5 \pm 7.6\%$) (Figure 1B, light gray vs green). Similarly, the percentage of PFKL-mEGFP-expressing Hs578T cells in the G1 phase was also increased by 13.4%, compared to the G1 population of asynchronous but PFKL-mEGFP-expressing cells (i.e., $52.5 \pm 3.2\%$ to $65.9 \pm 3.2\%$) (Figure 1C, red vs green). As anticipated, the treatment with thymidine showed a similar trend as the treatment of lovastatin with comparable degrees of increasing the G1 population regardless of the expression of the glucosome marker (blue vs green in Figure 1B,C).

Third, we blocked cell cycle progression in the G2/M phase using colchicine (100 nM) that disrupts an interaction between α - and β -tubulin for microtubule polymerization and thus interrupts the G2/M transition (Figure 1A).^{31–35} Our data showed that in the absence of the glucosome marker, the percentage of Hs578T cells in the G2 phase was increased by 25.1% relative to the percentage of asynchronous Hs578T cells in the G2 phase (i.e., $24.0 \pm 3.9\%$ to $49.1 \pm 3.4\%$) (Figure 1B, light gray vs black). In the presence of the glucosome marker, the percentage of Hs578T cells in the G2 phase was also increased 15.6% relative to the G2-arrested percentage of asynchronous Hs578T cells (i.e., $24.2 \pm 6.6\%$ to $39.8 \pm 4.9\%$) (Figure 1C, red vs black). Regardless of the expression of the glucosome marker, a significant percentage of Hs578T cells was arrested in the G2 phase by the treatment with colchicine.

Taken all together, we demonstrated that Hs578T cells that express PFKL-mEGFP as a glucosome marker went through the cell cycle in a very similar way as nontransfected Hs578T cells did. Therefore, these results allow us to investigate the changes in the metabolic state of glucose metabolism during the cell cycle in living human cells.

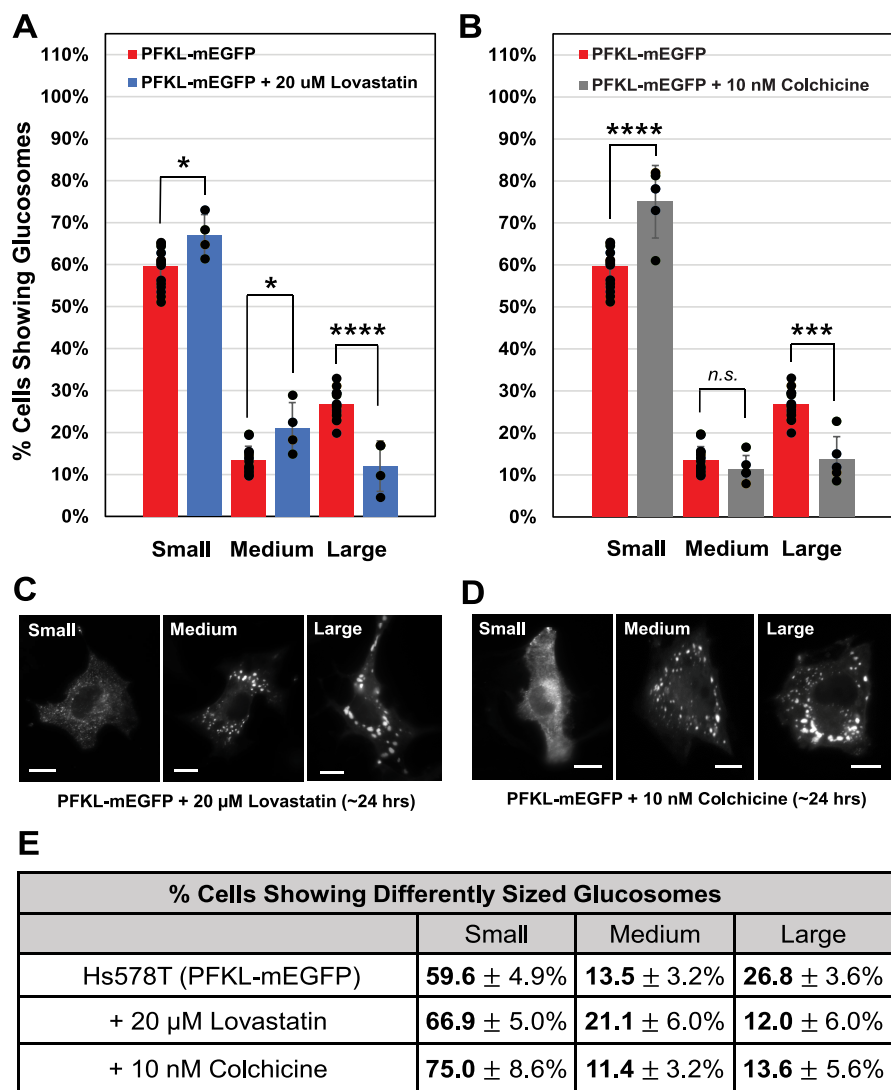


Figure 2. Effects of lovastatin and colchicine on cell population showing differently sized glucosomes. Population (%) of Hs578T cells displaying each size of PFKL-mEGFP assemblies was analyzed in the absence ($N = 14$) and presence ($N_{\text{lovastatin}} = 4$ and $N_{\text{colchicine}} = 5$) of 20 μ M lovastatin (A) and 10 nM colchicine (B), respectively. Statistical analyses were performed using two-way ANOVA and Tukey’s multiple comparison tests. Error bars represent standard deviations. Statistical significance is defined as $p < 0.05$ with a 95% confidence interval. * $p < 0.05$, *** $p < 0.001$, **** $p < 0.0001$. n.s., not significant. (C, D) Representative images obtained from inhibitor-treated Hs578T cells displaying three different sizes of glucosomes. Scale bars, 10 μ m. (E) Average percentages (%) of cells displaying differently sized glucosomes along with their standard deviations (\pm). Note that the concentrations of the cell cycle inhibitors we used for fluorescence live-cell imaging are lower, but still in the range of their concentrations being used in the literature,^{23–25,27,31–33,35} than what we used for flow cytometry in Figure 1.

Impacts of the Cell Cycle Inhibitors on Cell Population Showing Differently Sized Glucosomes

Now, to understand the impacts of the cell cycle inhibitors on glucosome assemblies at single-cell levels, we analyzed the percentage of Hs578T cells displaying different sizes of glucosomes in the absence and presence of lovastatin and colchicine, respectively. First, our high-content imaging analysis with lovastatin (20 μ M) revealed that the population of Hs578T cells showing large-sized glucosomes drastically decreased from 26.8% \pm 3.6 to 12.0 \pm 6.0% (Figure 2A,C,E). The population of cells showing small- and medium-sized glucosomes concurrently increased after the treatment with lovastatin, 59.6 \pm 4.9% to 66.9 \pm 5.0% and 13.5 \pm 3.2% to 21.1 \pm 6.0%, respectively. In addition, when colchicine (10 nM) was added to arrest Hs578T cells in the G2 phase, the population of Hs578T cells showing large-sized glucosomes

significantly decreased as well from 26.8 \pm 3.6% to 13.6 \pm 5.6% (Figure 2B,D,E). The population of Hs578T cells showing small-sized glucosomes was then significantly increased from 59.6 \pm 4.9% to 75.0 \pm 8.6% by colchicine. However, no change in the population of cells showing medium-sized glucosomes was observed (i.e., 13.5 \pm 3.2% vs 11.4 \pm 3.2%) with colchicine. Please note that none of the Hs578T cells we have analyzed under fluorescence single-cell imaging, including the cells with large-sized glucosomes, showed any observable distress before or after the inhibitor treatment under brightfield imaging.

These data revealed that the treatment with colchicine modulated glucosomes similarly to the treatment with lovastatin although their mechanisms of action are significantly different: that is, lovastatin arrests cells in the G1 phase through the inhibition of a metabolic enzyme (i.e., 3-hydroxy-

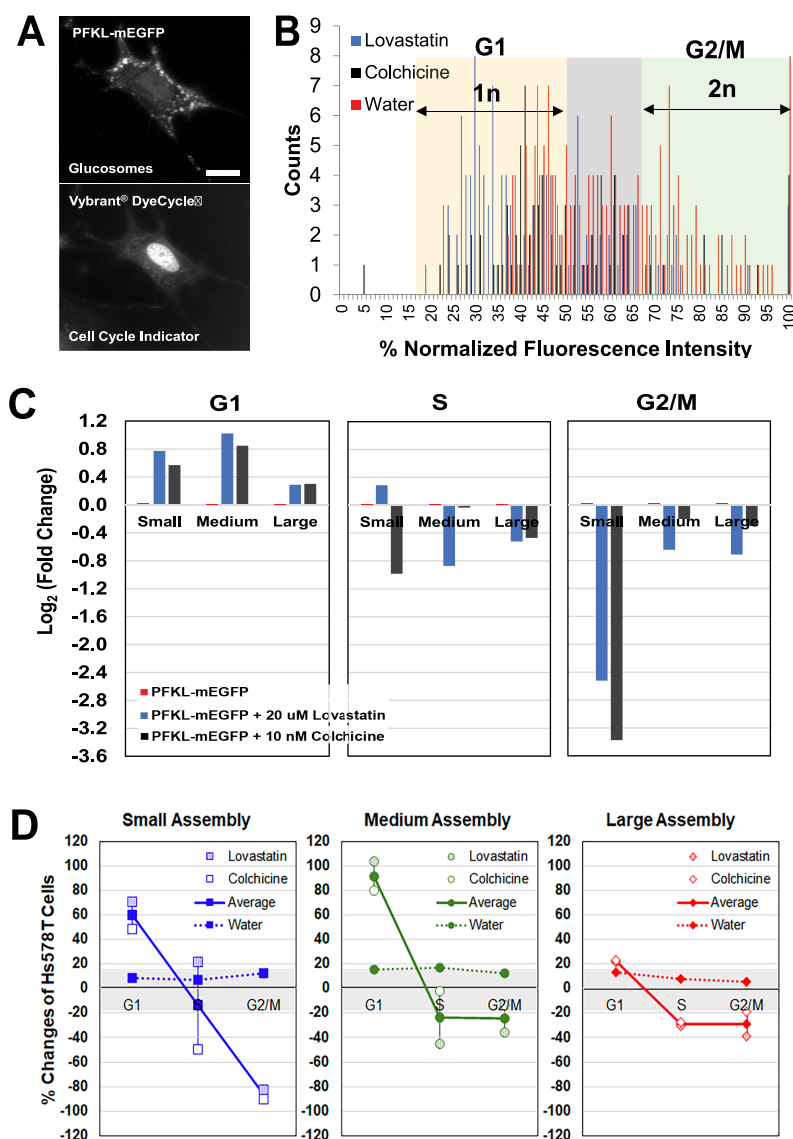


Figure 3. Size-dependent regulation of glucosomes during the cell cycle in single cells. (A) Representative Hs578T cell expressing PFKL-mEGFP in the cytoplasm was stained with a cell cycle indicator, Vybrant DyeCycle Orange Stain, that localized in the nucleus. Scale bars, 10 μm . (B) Total of 398 cells that displayed both glucosomes and the cell cycle indicator were randomly selected for analysis: $N_{\text{lovastatin}} = 141$ from 3 independent trials, $N_{\text{colchicine}} = 85$ from 4 independent trials, and $N_{\text{vehicle}} = 172$ from 7 independent trials. A histogram of the selected cells was then graphed as the number of counted cells over the normalized fluorescence intensity. Accordingly, the $1n$ group represents Hs578T cells in the G1 phase while the $2n$ group represents Hs578T cells in the G2 phase. (C) Changes of the population of Hs578T cells displaying each size of glucosomes were analyzed in the presence of either lovastatin (blue) or colchicine (black) at each phase of the cell cycle. Out of 226 inhibitor-treated Hs578T cells, $N_{\text{G1}} = 138$ cells, $N_{\text{S}} = 55$ cells, and $N_{\text{G2/M}} = 33$ cells were analyzed. A logarithmic value of fold changes (i.e., $\text{Log}_2(\text{fold change})$) of the population of cells showing different sizes of glucosomes are graphed relative to a control (red, $y = 0$). (D) Percentage (%) changes of cells showing small- (blue, square), medium- (green, circle), and large-sized (red, diamond) glucosomes were analyzed along with the cell cycle in the presence of lovastatin (shaded symbols) or colchicine (open symbols). The average (%) changes of cells by two cell cycle inhibitors were then graphed in a size-dependent manner (filled symbols with solid lines). Background changes were also observed by the treatment of a vehicle, water, as a control (filled symbols with dashed lines). Positive and negative (%) values on the y -axis indicate up- and down-regulation of the percentage of cells showing given sized glucosomes, respectively. The gray zone ($\pm 17\%$ on the y -axis) indicates background noise observed by the water treatment in this analysis. Note that graphs in panels C and D do not show error bars because the 398 cells that were randomly collected from 14 independent trials were individually analyzed with respect to their cell cycle and glucosome utilization. In addition, for clarity, we added a line between two data points obtained from each cell cycle inhibitor to indicate fluctuation ranges of data points.

3-methylglutaryl coenzyme A reductase) in cholesterol synthesis^{24,26} while colchicine interrupts the G2/M transition by disrupting the formation of microtubules.^{32,36} Considering that changes of cell population showing different sizes of glucosomes have been indicative of metabolic alterations of the subjected cell population,^{15,19–21} our data in Figure 2 likely

resulted from a similar biological response that was affected by both molecules. In other words, the changes in cells showing differently sized glucosomes in a population (Figure 2) appear to be independent of the individual mechanism of action of lovastatin or colchicine. Therefore, we hypothesized that a

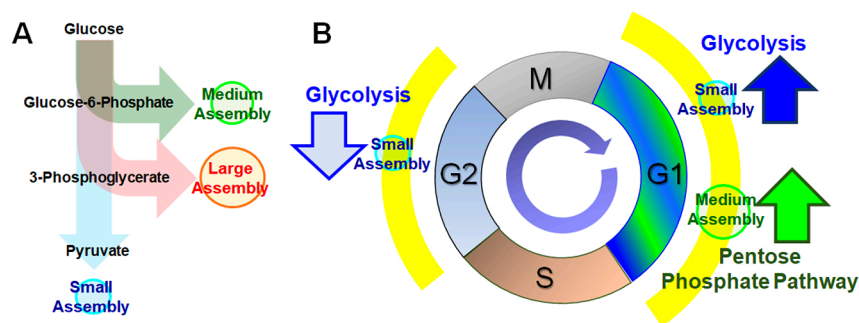


Figure 4. Functional interpretation of glucosome dynamics during the cell cycle. (A) Schematic diagram of our proposed size-dependent functional roles of glucosomes in glucose metabolism,^{15,19,20} indicating that small-sized glucosomes primarily promote glycolysis, but medium- and large-sized glucosomes partition glucose flux preferentially into the pentose phosphate pathway and serine biosynthesis, respectively. (B) Schematic diagram of size-dependent functional contributions of glucosomes during the cell cycle.

specific phase of the cell cycle may be the key determinant for the observed glucosome utilization in single cells.

Size-Dependent Distribution of Glucosomes at Specific Phases of the Cell Cycle in Single Cells

Next, to investigate whether a specific phase of the cell cycle is responsible for regulating glucosome assemblies at single-cell levels, we introduced a fluorescent cell cycle indicator, Vybrant DyeCycle Orange Stain (0.5 μM),^{37–41} to Hs578T cells that expressed PFKL-mEGFP as a glucosome marker (Figure 3A). We then randomly selected Hs578T cells displaying glucosomes in the presence of lovastatin ($N_{\text{lovastatin}} = 141$) and colchicine ($N_{\text{colchicine}} = 85$), respectively. Subsequently, fluorescent intensities of the cell cycle indicator were quantified from the nucleus of the selected cells to determine at which phase of the cell cycle they were. As a control, we also analyzed a number of glucosome-displaying cells ($N_{\text{vehicle}} = 172$) after treatment with water. Consequently, a histogram was set for our in-depth cell cycle analysis (Figure 3B) as described in the Materials and Methods section.

When we analyzed the randomly selected Hs578T cells after the treatment with lovastatin and colchicine, respectively, we found that the numbers of inhibitor-treated Hs578T cells that are arrested in the G1 phase, regardless of the cells showing small-, medium-, or large-sized glucosomes, were increased relative to the numbers of vehicle-treated Hs578T cells in the G1 phase (Figure 3C and Supplemental Figure S2A,D, from red to blue or black). Although one specific size of glucosome was not distinctively controlled by the G1 phase, the number of Hs578T cells showing small- and medium-sized glucosomes in the G1 phase were noticeably increased by lovastatin as well as by colchicine (Figure 3C and Supplemental Figure S2A,D, red to blue or black). However, the numbers of Hs578T cells in the G2/M phase, regardless of glucosome sizes, were decreased in the presence of lovastatin or colchicine (Figure 3C and Supplemental Figure S2C,F, red to blue or black). Particularly, significant reduction of the number of G2/M-arrested Hs578T cells was observed when cells displayed small-sized glucosomes after each inhibitor treatment (Figure 3C and Supplemental Figure S2C,F). The up- and down-regulation trends we observed with lovastatin at each phase of the cell cycle (Figure 3C, blue) were very similar to the trends we observed with colchicine (Figure 3C, black), except for the cells in the S phase. Therefore, the changes of glucosome utilization in single cells appears to depend on at which phase of the cell cycle a cell is during cell cycle progression.

Size-Specific Dynamics of Glucosomes during the Cell Cycle

To advance our understanding of the size-specific dynamics of glucosomes during the cell cycle, we have further analyzed our data shown in Figure 3C. Regardless of the treatment with lovastatin or colchicine, we found consistently that on average the percentage of cells showing small-sized glucosomes in the G1 phase increased 60% while the percentage of cells showing small-sized glucosomes in the G2/M phase significantly decreased 86% (Figure 3D). This suggests that small-sized glucosomes are most dynamically associated with the cell cycle, suggesting their potential oscillatory behavior during cell cycle progression. Meanwhile, the percentage of cells showing medium-sized glucosomes was significantly elevated only in the G1 phase (i.e., on average 90%) (Figure 3D), which suggests the importance of medium-sized glucosomes during the G1 phase. Lastly, the percentage of cells showing large-sized glucosomes was barely or only minimally changed during the cell cycle (Figure 3D), indicating that utilization of large-sized glucosomes remains relatively constant throughout the cell cycle. If we put these data together in multiple cycles repeatedly, our results seem to suggest that the percentages of cells showing glucosomes may oscillate along with the cell cycle in an assembly size-specific manner. Therefore, we disclose intracellular glucosome dynamics as a possible mechanism by which human cells regulate glucose metabolism during the cell cycle.

DISCUSSION

Previously, we have proposed the size-dependent functional participation of glucosome assemblies in regulation of glucose flux at single-cell levels (Figure 4A); briefly, small-sized glucosomes primarily promote glycolysis,^{19,20} but medium- and large-sized glucosomes partition glucose flux preferentially into the PPP and serine biosynthesis, respectively.^{15,20} This means that the significantly increased numbers of Hs578T cells showing small- and medium-sized glucosomes in the G1 phase (Figure 3C,D) may represent the metabolic upregulation of glycolysis and the PPP during the G1 phase (Figure 4B). This is indeed consistent with the literature proposing that the increased expression of hexokinase 2 or PFKFB3, as well as the elevated activity of glucose 6-phosphate dehydrogenase, in the G1 phase would upregulate glycolysis and the PPP during the G1 phase, respectively.^{7,8,11,14} Our analysis here is also in line with the fact that human *de novo* purine biosynthesis, which relies on glucose-derived carbon flux from the PPP, is

upregulated in the G1 phase through the formation of multienzyme purinosome assemblies.³⁸ Additionally, the percentage of Hs578T cells showing medium- and large-sized glucosomes from the S to the G2/M phase (Figure 3D) remained almost the same, indicating no alteration of the glucose shunt to building block biosynthesis. In other words, our data seems to suggest a relatively sustained level of glycolysis-derived carbon flux into the PPP and serine biosynthesis during the S to G2/M transition. This analysis is appealing because we provide a mechanistic insight of how serine is continually generated in cancer cells to play its reported essential role in cancer cell growth and survival.^{42,43} Furthermore, our data showing reduced amounts of small-sized glucosomes in the G2/M-arrested cells (Figure 3C,D) implies significant downregulation of glycolysis at the G2 phase of Hs578T cells (Figure 4B). Although the activity of glycolysis is shown to diminish during the S phase relative to its level at the G1 phase,^{6,44} as far as we know, glycolysis has not been previously reported to be downregulated during the G2 phase relative to its basal level activity throughout the cell cycle. In addition, the downregulation of glycolysis in the G2 phase (Figures 3D and 4B) with no significant changes on glucose flux shunting to the PPP and serine biosynthesis (Figure 3D) may indicate glycolytic intermediates, particularly dihydroxyacetone phosphate, leaking to lipid metabolism,⁴⁵ which may explain the upregulation of lipid biosynthesis during the G2.⁴⁶ Collectively, our study not only strongly supports our current understanding of metabolic demands in the G1 phase but also provides novel insights into functional interplays between glucose metabolism and the G2 phase of the cell cycle in human cells.

In addition, it is important to note here that a current model that describes temporal oscillation of metabolism during cell cycle progression has been largely established from yeast and unicellular eukaryotic cells.⁶ Particularly, metabolite profiling experiments in yeast cells demonstrated periodic changes of intracellular concentrations of metabolites, thus revealing metabolic oscillation during the cell cycle.⁴⁷ In human cells, however, recent research has been largely centered on elucidating the impacts of cyclin-dependent kinases on the spatial translocation of glycolytic enzymes (e.g., pyruvate kinase muscle-type 2 (PKM2), aldolase, glyceraldehyde 3-phosphate dehydrogenase, and PFKFB3) from the cytoplasm to the nucleus,⁵ rather than monitoring changes in their enzymatic activities during the cell cycle. Nonetheless, there is a study indeed demonstrating the diversion of glycolytic flux toward building block biosynthesis in cancer cells due to the alterations of enzymatic activities of glycolytic enzymes (i.e., PFK and PKM2) by cyclin-dependent kinase 6.⁴⁸ Our understanding of whether functional oscillation of metabolic pathways occurs during the cell cycle in human cells is about to be emerging.

Overall, we demonstrate that glucosomes are spatially and temporally regulated at single-cell levels and that the percentages of cells showing a specific size of glucosomes are modulated during the cell cycle in a glucosome size-specific manner. We propose that glucosome dynamics is one of the essential metabolic entities of human cell biology to meet the cell cycle-dependent metabolic demands of human cells.

MATERIALS AND METHODS

Materials

The plasmid expressing PFKL with a monomeric enhanced green fluorescent protein (PFKL-mEGFP) was previously described.¹⁵ Thymidine (Sigma, Cat# 89270), colchicine (EMD Millipore, Cat# 234115), and lovastatin (Tocris, Cat# 1530) were used to synchronize Hs578T cells.³⁰ Vybrant DyeCycle Orange Stain (Invitrogen, Cat# V35005) was used as a cell cycle indicator. Note that lovastatin was first dissolved in 95% ethanol, and then 1 M NaOH was added. Subsequently, the pH of the lovastatin solution was adjusted to pH 7.2 using 1 M HCl, followed by diluting it with water to prepare a desired stock solution.

Cell Culture

Human triple-negative breast carcinoma Hs578T cells (HTB-126) were obtained from the ATCC. Cells were cultured in Roswell Park Memorial Institute 1640 (RPMI 1640, Mediatech, Cat# 10-040-CV) supplemented with 10% dialyzed fetal bovine serum (dFBS) (Sigma, Cat# F2442)^{49,50} and 50 μ g/mL gentamicin sulfate (Corning, Cat# 61-098-RF). Cells were then maintained in a HeraCell CO₂ incubator (37 °C, 5% CO₂, and 95% humidity). The Universal Mycoplasma Detection Kit (ATCC, Cat# 30-1012K) was used to verify that cells were free of mycoplasma contamination. The Hs578T cell line was also authenticated by ATCC's short tandem repeat profiling service.

Transfection

Hs578T cells were gently removed from a culture flask with trypsin (Corning, Cat# 25-053-Cl) and plated on glass-bottomed 35 mm Petri dishes (MatTek) with an antibiotic-free growth medium. When cells reached ~70–90% confluency, transfection was carried out using Lipofectamine 2000 (Invitrogen) with Opti-MEM-I reduced serum medium (Gibco, Cat# 11058). At 5 h post-transfection, the Opti-MEM-I medium was exchanged with a fresh antibiotic-free growth medium that did not contain phenol red (Gibco, Cat# 11835-030) but, when desired, included a cell cycle inhibitor.

Cell Synchronization

Hs578T cells were grown in 6-well plates ~30–50% confluency in the growth medium (i.e., RPMI 1640 and 10% dFBS). On the following day, cells were transfected with PFKL-mEGFP. Cells with or without PFKL-mEGFP were treated with thymidine, lovastatin, or colchicine.^{29,30} For the G1/S arrest, 2 mM thymidine was added into the growth medium. After 12 h of incubation, cells were washed with 1× PBS twice and subsequently incubated with the fresh growth medium for 16 h. Thymidine treatment was then repeated (2 mM thymidine for 12 h) before harvesting cells. For the G1 arrest, 40 μ M lovastatin was supplemented into the growth medium. After 28 h of incubation, cells were washed with the fresh growth medium to remove residual lovastatin. For the G2/M arrest, 100 nM colchicine was supplemented into the growth medium for 24 h. For the vehicle control, water was applied without a cell cycle inhibitor.

Flow Cytometric Analysis

Cells were then harvested and analyzed by flow cytometry.⁵¹ Briefly, cells were removed from a culture plate using trypsin and washed with 1× PBS once. Then, the cells were resuspended in ice-cold 1× PBS and fixed in ice-cold methanol for 20 min at 4 °C. The cells were washed and resuspended with 1× PBS containing 30 μ g/mL propidium iodide and 100 μ g/mL RNase A (Thermo, Cat# EN0531). After incubation for at least 45 min, cells were subjected to flow cytometry using a CyAn ADP instrument (Beckman Coulter) equipped with a 488 nm laser line and 530/40 and 613/20 emission filters with Summit V 4.00 software. The cell population was gated based on mEGFP intensity to exclude cells that were not expressing PFKL-mEGFP. Using the Cell Cycle platform available in FlowJo (FlowJo, LLC), cell cycle progression was determined by Dean–Jett–Fox analysis.⁵²

Fluorescence Live-Cell Imaging

At 24 h post-transfection of PFKL-mEGFP, Hs578T cells were washed with a buffered-saline solution (20 mM HEPES (pH 7.4), 135

mM NaCl, 5 mM KCl, 1 mM MgCl₂, 1.8 mM CaCl₂, and 5.6 mM glucose) three times in a 10 min interval. To employ a cell cycle indicator, cells were subsequently treated with Vybrant DyeCycle Orange Stain (0.5 μ M) for 15 min (37 °C, 5% CO₂, and 95% humidity) and allowed to further incubate in the darkroom for 1–2 h at ambient temperature prior to imaging. All images were obtained using a Photometrics CoolSnap EZ monochrome CCD camera with a 60 \times 1.45 NA objective (Nikon CFI Plan Apo TIRF) on a Nikon Eclipse Ti inverted C2 confocal microscope. Wide-field imaging was carried out using a set of Z488/10-HC cleanup, HC TIRF dichroic, and 525/50-HC emission filter for mEGFP detection and a set of Z561/10-HC cleanup, HC TIRF dichroic, and 600/50-HC emission filter for the Vybrant DyeCycle Orange Stain detection from Chroma Technology.

Glucosome Size Analysis

The ImageJ processing software (National Institutes of Health) was used for glucosome size analysis as reported previously.¹⁵ Briefly, fluorescent wide-field images were processed through ImageJ using a custom script and macro that automate the counting of fluorescent particles using its built-in module, so-called robust automatic threshold selection (RATS). Note that the captured cell images were scaled according to the pixel size of the microscope (i.e., 0.12 μ m/pixel) before the default parameters for RATS (i.e., noise threshold = 25, λ factor = 3) were used in this analysis. Once fluorescent particles were selected from an image, the particle analysis module in ImageJ was applied to attain both the number and the area of fluorescent particles within an image. This process was repeated for all subsequent cell images.

Fluorescent Intensity Analysis from Cell Cycle Indicator

The cell cycle indicator Vybrant DyeCycle Orange Stain emits fluorescent signals that are proportional to the mass of DNA in single cells, which indicates cell cycle progression.^{37–41} To distinguish each phase of the cell cycle based on a fluorescent intensity from the nucleus, Nikon NIS-Elements software (version 4.13) was used to quantify fluorescent signals from single cells. Cells emitting the highest fluorescent intensity served as a reference for the G2/M-arrested cells. Cells in the G1 phase were then characterized as having half of the reference fluorescence intensity. Any cells with a fluorescence intensity between the G1 and G2/M phases were categorized as being in the S phase.

Statistical Analysis

Statistical analyses of high-content imaging and flow cytometry data were performed by using GraphPad Prism 9.2. Briefly, a two-way analysis of variance (ANOVA) with Tukey's multiple comparison tests was performed to determine statistical significance among different treatments or between the experimental and the control groups. Statistical significance was defined as $p < 0.05$ with a 95% confidence interval: * $p < 0.05$, ** $p < 0.01$, *** $p < 0.001$, **** $p < 0.0001$; n.s., not significant.

■ ASSOCIATED CONTENT

Data Availability Statement

All data are available within the main manuscript and the [Supporting Information](#).

SI Supporting Information

The Supporting Information is available free of charge at <https://pubs.acs.org/doi/10.1021/acsbiomedchemau.3c00037>.

Cell cycle analysis with and without expression of a glucosome marker, PFKL-mEGFP, in Hs578T cells; changes of the population of Hs578T cells displaying three different sizes of glucosomes at each phase of the cell cycle ([PDF](#))

■ AUTHOR INFORMATION

Corresponding Author

Songon An – Department of Chemistry and Biochemistry, University of Maryland Baltimore County (UMBC), Baltimore, Maryland 21250, United States; Program in Oncology, Marlene and Stewart Greenebaum Comprehensive Cancer Center, University of Maryland, Baltimore, Maryland 21201, United States; orcid.org/0000-0003-2189-7374; Email: san@umbc.edu

Authors

Miji Jeon – Department of Chemistry and Biochemistry, University of Maryland Baltimore County (UMBC), Baltimore, Maryland 21250, United States

Danielle L. Schmitt – Department of Chemistry and Biochemistry, University of Maryland Baltimore County (UMBC), Baltimore, Maryland 21250, United States; Present Address: D.L.S.: Department of Chemistry and Biochemistry, University of California, Los Angeles, CA 90095, United States; orcid.org/0000-0002-7343-2125

Minjoung Kyoung – Department of Chemistry and Biochemistry, University of Maryland Baltimore County (UMBC), Baltimore, Maryland 21250, United States; Program in Oncology, Marlene and Stewart Greenebaum Comprehensive Cancer Center, University of Maryland, Baltimore, Maryland 21201, United States

Complete contact information is available at: <https://pubs.acs.org/10.1021/acsbiomedchemau.3c00037>

Author Contributions

S.A. conceived the project, M.J. and D.L.S. performed experiments, and M.J., D.L.S., and M.K. carried out statistical analysis. All authors analyzed and discussed the results and wrote the manuscript. CRediT: **Miji Jeon** data curation (lead), formal analysis (lead), investigation (lead), methodology (lead), visualization (equal), writing-original draft (lead), writing-review & editing (supporting); **Danielle L. Schmitt** data curation (equal), formal analysis (equal), investigation (supporting), visualization (equal), writing-review & editing (supporting); **Minjoung Kyoung** formal analysis (supporting), funding acquisition (lead), supervision (equal), writing-review & editing (equal); **Songon An** conceptualization (lead), data curation (lead), formal analysis (lead), funding acquisition (lead), project administration (lead), supervision (lead), writing-review & editing (lead).

Notes

The authors declare no competing financial interest.

■ ACKNOWLEDGMENTS

We thank Dr. Gregory Szeto's group at UMBC for their assistance in operation of flow cytometry. This work is supported by the National Institutes of Health: R01GM125981 (S.A.), R03CA219609 (S.A.), R01GM134086 (M.K.) and T32GM066706 (M.J., D.L.S.). The content is solely the responsibility of the authors and does not necessarily represent the official views of the National Institutes of Health.

■ REFERENCES

- (1) Cai, L.; Tu, B. P. Driving the cell cycle through metabolism. *Annu. Rev. Cell Dev Biol.* **2012**, *28*, 59–87.

- (2) Lee, I. H.; Finkel, T. Metabolic regulation of the cell cycle. *Curr. Opin. Cell Biol.* **2013**, *25*, 724–729.
- (3) Kalucka, J.; Missaen, R.; Georgiadou, M.; Schoors, S.; Lange, C.; De Bock, K.; Dewerchin, M.; Carmeliet, P. Metabolic control of the cell cycle. *Cell Cycle* **2015**, *14*, 3379–3388.
- (4) Roy, D.; Sheng, G. Y.; Herve, S.; Carvalho, E.; Mahanty, A.; Yuan, S.; Sun, L. Interplay between cancer cell cycle and metabolism: challenges, targets and therapeutic opportunities. *Biomed Pharmacother* **2017**, *89*, 288–296.
- (5) Icard, P.; Fournel, L.; Wu, Z.; Alifano, M.; Lincet, H. Interconnection between metabolism and cell cycle in cancer. *Trends Biochem. Sci.* **2019**, *44*, 490–501.
- (6) Kaplon, J.; van Dam, L.; Peeper, D. Two-way communication between the metabolic and cell cycle machineries: the molecular basis. *Cell Cycle* **2015**, *14*, 2022–2032.
- (7) Chen, J.; Zhang, S.; Li, Y.; Tang, Z.; Kong, W. Hexokinase 2 overexpression promotes the proliferation and survival of laryngeal squamous cell carcinoma. *Tumour Biol.* **2014**, *35*, 3743–3753.
- (8) Hu, J. W.; Sun, P.; Zhang, D. X.; Xiong, W. J.; Mi, J. Hexokinase 2 regulates G1/S checkpoint through CDK2 in cancer-associated fibroblasts. *Cell Signal* **2014**, *26*, 2210–2216.
- (9) Duan, S.; Pagano, M. Linking metabolism and cell cycle progression via the APC/CCdh1 and SCFbetaTrCP ubiquitin ligases. *Proc. Natl. Acad. Sci. U. S. A.* **2011**, *108*, 20857–20858.
- (10) Jia, W.; Zhao, X.; Zhao, L.; Yan, H.; Li, J.; Yang, H.; Huang, G.; Liu, J. Non-canonical roles of PFKFB3 in regulation of cell cycle through binding to CDK4. *Oncogene* **2018**, *37*, 1685–1698.
- (11) Peng, F.; Li, Q.; Sun, J. Y.; Luo, Y.; Chen, M.; Bao, Y. PFKFB3 is involved in breast cancer proliferation, migration, invasion and angiogenesis. *Int. J. Oncol.* **2018**, *52*, 945–954.
- (12) Shi, L.; Pan, H.; Liu, Z.; Xie, J.; Han, W. Roles of PFKFB3 in cancer. *Signal Transduct Target Ther* **2017**, *2*, 17044.
- (13) Benito, A.; Polat, I. H.; Noe, V.; Ciudad, C. J.; Marin, S.; Cascante, M. Glucose-6-phosphate dehydrogenase and transketolase modulate breast cancer cell metabolic reprogramming and correlate with poor patient outcome. *Oncotarget* **2017**, *8*, 106693–106706.
- (14) Vizán, P.; Alcarraz-Vizán, G.; Diaz-Moralli, S.; Solovjeva, O. N.; Frederiks, W. M.; Cascante, M. Modulation of pentose phosphate pathway during cell cycle progression in human colon adenocarcinoma cell line HT29. *Int. J. Cancer* **2009**, *124*, 2789–2796.
- (15) Kohnhorst, C. L.; Kyoung, M.; Jeon, M.; Schmitt, D. L.; Kennedy, E. L.; Ramirez, J.; Bracey, S. M.; Luu, B. T.; Russell, S. J.; An, S. Identification of a multienzyme complex for glucose metabolism in living cells. *J. Biol. Chem.* **2017**, *292*, 9191–9203.
- (16) Kyoung, M.; Russell, S. J.; Kohnhorst, C. L.; Esemoto, N. N.; An, S. Dynamic architecture of the purinosome involved in human de novo purine biosynthesis. *Biochemistry* **2015**, *54*, 870–880.
- (17) Jin, M.; Fuller, G. G.; Han, T.; Yao, Y.; Alessi, A. F.; Freeberg, M. A.; Roach, N. P.; Moresco, J. J.; Karnovsky, A.; Baba, M.; Yates, J. R., 3rd; Gitler, A. D.; Inoki, K.; Klionsky, D. J.; Kim, J. K. Glycolytic Enzymes Coalesce in G Bodies under Hypoxic Stress. *Cell Rep* **2017**, *20*, 895–908.
- (18) Webb, B. A.; Dosey, A. M.; Wittmann, T.; Kollman, J. M.; Barber, D. L. The glycolytic enzyme phosphofructokinase-1 assembles into filaments. *J. Cell Biol.* **2017**, *216*, 2305–2313.
- (19) Kennedy, E. L.; Jeon, M.; Augustine, F.; Chauhan, K. M.; An, S.; Kyoung, M. Functional regulation of 4D metabolic network between multienzyme glucosome condensates and mitochondria in living cells. *bioRxiv* **2022**, DOI: 10.1101/2022.05.16.491844.
- (20) Jeon, M.; Kang, H. W.; An, S. A mathematical model for enzyme clustering in glucose metabolism. *Sci. Rep* **2018**, *8*, 2696.
- (21) Jeon, M.; Chauhan, K. M.; Szeto, G. L.; Kyoung, M.; An, S. Subcellular regulation of glucose metabolism through multienzyme glucosome assemblies by EGF-ERK1/2 signaling pathways. *J. Biol. Chem.* **2022**, *298*, 101675.
- (22) Schmitt, D. L.; Dranchak, P.; Parajuli, P.; Blivis, D.; Voss, T.; Kohnhorst, C. L.; Kyoung, M.; Inglese, J.; An, S. High-content quantitative high-throughput screening identifies a cell cycle-associated signaling cascade that regulates a multienzyme metabolic assembly for glucose metabolism. *bioRxiv* **2022**, DOI: 10.1101/2022.06.10.495654.
- (23) Carcelen, M.; Vidal, V.; Franco, A.; Gomez, M.; Moreno, F.; Fernandez-Luna, J. L. Plasmonic Biosensing for Label-Free Detection of Two Hallmarks of Cancer Cells: Cell-Matrix Interaction and Cell Division. *Biosensors (Basel)* **2022**, *12*, 674.
- (24) Laurent, J.; Frongia, C.; Cazales, M.; Mondesert, O.; Ducommun, B.; Lobjois, V. Multicellular tumor spheroid models to explore cell cycle checkpoints in 3D. *BMC Cancer* **2013**, *13*, 73.
- (25) Shibata, M. A.; Kavanaugh, C.; Shibata, E.; Abe, H.; Nguyen, P.; Otsuki, Y.; Trepel, J. B.; Green, J. E. Comparative effects of lovastatin on mammary and prostate oncogenesis in transgenic mouse models. *Carcinogenesis* **2003**, *24*, 453–459.
- (26) Abukhdeir, A. M.; Park, B. H. P21 and p27: roles in carcinogenesis and drug resistance. *Expert Rev. Mol. Med.* **2008**, *10*, No. e19.
- (27) Wu, J. R.; Gilbert, D. M. Lovastatin arrests CHO cells between the origin decision point and the restriction point. *FEBS Lett.* **2000**, *484*, 108–112.
- (28) Zhang, X.; Teng, Y.; Yang, F.; Wang, M.; Hong, X.; Ye, L. G.; Gao, Y. N.; Chen, G. Y. MCM2 is a therapeutic target of lovastatin in human non-small cell lung carcinomas. *Oncol. Rep.* **2015**, *33*, 2599–2605.
- (29) Chen, G.; Deng, X. Cell synchronization by double thymidine block. *Bio Protoc* **2018**, *8*, No. e2994.
- (30) Jackman, J.; O'Connor, P. M. Methods for synchronizing cells at specific stages of the cell cycle. *Curr. Protoc Cell Biol.* **2001**, *8.3.1*.
- (31) Kim, S.-K.; Cho, S.-M.; Kim, H.; Seok, H.; Kim, S.-O.; Kyu Kwon, T.; Chang, J.-S. The colchicine derivative CT20126 shows a novel microtubule-modulating activity with apoptosis. *Exp. Mol. Med.* **2013**, *45*, No. e19.
- (32) Blajeski, A. L.; Phan, V. A.; Kottke, T. J.; Kaufmann, S. H. G(1) and G(2) cell-cycle arrest following microtubule depolymerization in human breast cancer cells. *J. Clin. Invest* **2002**, *110*, 91–99.
- (33) Chopra, A.; Bond, M. J.; Bleiler, M.; Yeagley, M.; Wright, D.; Giardina, C. Efficient Activation of Apoptotic Signaling during Mitotic Arrest with AK301. *PLoS One* **2016**, *11*, No. e0153818.
- (34) Jordan, M. A.; Toso, R. J.; Thrower, D.; Wilson, L. Mechanism of mitotic block and inhibition of cell proliferation by taxol at low concentrations. *Proc. Natl. Acad. Sci. U. S. A.* **1993**, *90*, 9552–9556.
- (35) Bhattacharya, S.; Das, A.; Datta, S.; Ganguli, A.; Chakrabarti, G. Colchicine induces autophagy and senescence in lung cancer cells at clinically admissible concentration: potential use of colchicine in combination with autophagy inhibitor in cancer therapy. *Tumour Biol.* **2016**, *37*, 10653–10664.
- (36) Li, L.; Jiang, S.; Li, X.; Liu, Y.; Su, J.; Chen, J. Recent advances in trimethoxyphenyl (TMP) based tubulin inhibitors targeting the colchicine binding site. *Eur. J. Med. Chem.* **2018**, *151*, 482–494.
- (37) Bedelbaeva, K.; Snyder, A.; Gourevitch, D.; Clark, L.; Zhang, X. M.; Leferovich, J.; Cheverud, J. M.; Lieberman, P.; Heber-Katz, E. Lack of p21 expression links cell cycle control and appendage regeneration in mice. *Proc. Natl. Acad. Sci. U. S. A.* **2010**, *107*, 5845–5850.
- (38) Chan, C. Y.; Zhao, H.; Pugh, R. J.; Pedley, A. M.; French, J.; Jones, S. A.; Zhuang, X.; Jinnah, H.; Huang, T. J.; Benkovic, S. J. Purinosome formation as a function of the cell cycle. *Proc. Natl. Acad. Sci. U. S. A.* **2015**, *112*, 1368–1373.
- (39) Dicker, D. T.; Lerner, J. M.; El-Deiry, W. S. Hyperspectral image analysis of live cells in various cell cycle stages. *Cell Cycle* **2007**, *6*, 2563–2570.
- (40) Zurek-Biesiada, D.; Szczurek, A. T.; Prakash, K.; Best, G.; Mohana, G. K.; Lee, H. K.; Roignant, J. Y.; Dobrucki, J. W.; Cremer, C.; Birk, U. Quantitative super-resolution localization microscopy of DNA in situ using Vybrant(R) DyeCycle Violet fluorescent probe. *Data Brief* **2016**, *7*, 157–171.
- (41) Zurek-Biesiada, D.; Szczurek, A. T.; Prakash, K.; Mohana, G. K.; Lee, H. K.; Roignant, J. Y.; Birk, U. J.; Dobrucki, J. W.; Cremer, C. Localization microscopy of DNA in situ using Vybrant(R) DyeCycle Violet fluorescent probe: A new approach to study nuclear

nanostructure at single molecule resolution. *Exp. Cell Res.* **2016**, *343*, 97–106.

(42) Chaneton, B.; Hillmann, P.; Zheng, L.; Martin, A. C. L.; Maddocks, O. D. K.; Chokkathukalam, A.; Coyle, J. E.; Jankevics, A.; Holding, F. P.; Vousden, K. H.; Frezza, C.; O'Reilly, M.; Gottlieb, E. Serine is a natural ligand and allosteric activator of pyruvate kinase M2. *Nature* **2012**, *491*, 458–462.

(43) Maddocks, O. D.; Berkers, C. R.; Mason, S. M.; Zheng, L.; Blyth, K.; Gottlieb, E.; Vousden, K. H. Serine starvation induces stress and p53-dependent metabolic remodelling in cancer cells. *Nature* **2013**, *493*, 542–546.

(44) Bao, Y.; Mukai, K.; Hishiki, T.; Kubo, A.; Ohmura, M.; Sugiura, Y.; Matsuura, T.; Nagahata, Y.; Hayakawa, N.; Yamamoto, T.; Fukuda, R.; Saya, H.; Suematsu, M.; Minamishima, Y. A. Energy management by enhanced glycolysis in G1-phase in human colon cancer cells in vitro and in vivo. *Mol. Cancer Res.* **2013**, *11*, 973–985.

(45) Otto, A. M. Small is beautiful—a glycolytic metabolite signals mTORC1 activation in cancer cell metabolism. *Signal Transduct Target Ther* **2020**, *5*, 259.

(46) da Veiga Moreira, J.; Peres, S.; Steyaert, J. M.; Bigan, E.; Pauleve, L.; Nogueira, M. L.; Schwartz, L. Cell cycle progression is regulated by intertwined redox oscillators. *Theor Biol. Med. Model* **2015**, *12*, 10.

(47) Tu, B. P.; Mohler, R. E.; Liu, J. C.; Dombek, K. M.; Young, E. T.; Synovec, R. E.; McKnight, S. L. Cyclic changes in metabolic state during the life of a yeast cell. *Proc. Natl. Acad. Sci. U. S. A.* **2007**, *104*, 16886–16891.

(48) Wang, H.; Nicolay, B. N.; Chick, J. M.; Gao, X.; Geng, Y.; Ren, H.; Gao, H.; Yang, G.; Williams, J. A.; Suski, J. M.; Keibler, M. A.; Sicinska, E.; Gerdemann, U.; Haining, W. N.; Roberts, T. M.; Polyak, K.; Gygi, S. P.; Dyson, N. J.; Sicinski, P. The metabolic function of cyclin D3-CDK6 kinase in cancer cell survival. *Nature* **2017**, *546*, 426–430.

(49) An, S.; Jeon, M.; Kennedy, E. L.; Kyoung, M. Phase-separated condensates of metabolic complexes in living cells: purinosome and glucosome. *Methods Enzymol* **2019**, *628*, 1–17.

(50) An, S.; Kumar, R.; Sheets, E. D.; Benkovic, S. J. Reversible compartmentalization of de novo purine biosynthetic complexes in living cells. *Science* **2008**, *320*, 103–106.

(51) Crowley, L. C.; Chojnowski, G.; Waterhouse, N. J. Measuring the DNA content of cells in apoptosis and at different cell-cycle stages by propidium iodide staining and flow cytometry. *Cold Spring Harb Protoc* **2016**, *2016*, 905–910.

(52) Fox, M. H. A model for the computer analysis of synchronous DNA distributions obtained by flow cytometry. *Cytometry* **1980**, *1*, 71–77.

Recommended by ACS

Digestibility of Malondialdehyde-Induced Dietary Advanced Lipoxidation End Products and Their Effects on Hepatic Lipid Accumulation in Mice

Yaya Wang, Shuo Wang, *et al.*

JUNE 30, 2023

JOURNAL OF AGRICULTURAL AND FOOD CHEMISTRY

READ 

Dynamic Control of Functional Coacervates in Synthetic Cells

Karthika S. Nair, Harsha Bajaj, *et al.*

JUNE 19, 2023

ACS SYNTHETIC BIOLOGY

READ 

Ca/Fe-Based Nanozymes Relieve Severe Acute Pancreatitis by Ferroptosis Regulation and Reactive Oxygen Species Scavenging

Yuhang Li, Sulai Liu, *et al.*

JULY 13, 2023

ACS APPLIED NANO MATERIALS

READ 

Mitochondrial-Derived Peptide MOTS-c Ameliorates Spared Nerve Injury-Induced Neuropathic Pain in Mice by Inhibiting Microglia Activation and Neuronal Oxidative...

Jinhong Jiang, Zhe Wang, *et al.*

JUNE 07, 2023

ACS CHEMICAL NEUROSCIENCE

READ 

Get More Suggestions >